Topographical changes caused by moderate and small floods in a gravelly ephemeral river - 2D morphodynamic simulation approach

Eliisa Lotsari[1, 5], Mikel Calle[2], Gerardo Benito[2], Antero Kukko[3, 4], Harri Kaartinen[3], Juha Hyyppä[3], Hannu Hyyppä[4] and Petteri Alho[3, 4, 5]

5 [1]Department of Geographical and Historical Studies, University of Eastern Finland, Joensuu, Yliopistokatu 2, P.O. Box 111, 80101 Joensuu, Finland
[2] National Museum of Natural Sciences, Spanish Research Council (CSIC), Madrid, Calle de Serrano 117, 28006 Madrid, Spain
[3] Department of Remote Sensing and Photogrammetry, Finnish Geospatial Research Institute, National Land Survey of
10 Finland, Kirkkonummi, Geodeetinrinne 2, 02430 Masala, Finland
[4] Department of Built Environment, Aalto University, Espoo, Vaisalantie 8, P.O.Box 15800, 00076 Aalto, Finland
[5] Department of Geography and Geology, University of Turku, Turku, 20014 Turun yliopisto, Finland

Correspondence to: Eliisa S. Lotsari (eliisa.lotsari@uef.fi)

Abstract. In ephemeral rivers, channel morphology represents a snapshot at the end of a succession of geomorphic changes
15 performed by a flood. In most cases, the channel shape and bedform evolution during different phases of a flood hydrograph are not recognized from field evidence. This paper analyzes the capabilities of morphodynamic modelling (Delft 2D) for resolving the evolution of a gravelly ephemeral river channel during consecutive, moderate- and low-magnitude discharge events. We pursue for schematic concepts for simulations in ephemeral gravely rivers that provide an outcome with the closest similarity to the post-flood reality. Based on the simulations, we analyze the morphodynamic evolution of Rambla de la Viuda
20 (Spain) to find out when and to what extent the channel changes occur during the phases of moderate- (March 2013) and low-magnitude (May 2013) discharge events, and what influence the discharge has on the rate of morphological changes. The model performance is examined with different parameterizations.

The spatially varying grain size data and transport equations were the most important factors, in addition to the quality of
25 recorded discharge, for the simulation results of the channel evolution. The total load equation worked better, compared to the deterministic equation. The erosion and deposition can be in total greater during the long-lasting receding phase than during the rising phase. The deposition and erosion peaks are predicted to occur at the beginning of the moderate-magnitude discharge event, whereas deposition dominates throughout the event. On the contrary, the low-magnitude discharge event only experiences the peak of channel changes after the discharge peak. These different predicted erosion/deposition patterns suggest
30 a hysteresis effect on the morphodynamic changes, and stress the importance of previous flood history (timing, succession and magnitude) in understanding the geomorphic response of gravelly ephemeral rivers.

1 Introduction

The hydrology of ephemeral rivers is dominated by occasional large flash floods that cause morphological fluvial changes (Tooth, 2000; Benito et al., 2011). Consequently, most geomorphological studies have been mainly concentrated on these greatest flow events, due to their impacts on the river channel changes, related river environments and human infrastructure

5 (Greenbaum and Bergman, 2006; Grodek et al., 2012; Nardi and Rinaldi, 2015; Hooke, 2016b). However, moderate and low flows have also been shown to cause great morphological changes in gravelly river channels (Calle et al., 2015; Hooke, 2016a), as a small discharge over long time spans can substantially rework the sediment and fluvial bedforms produced by the greater floods (Greenbaum and Bergman, 2006).

10 According to Hooke and Mant (2000), the pattern and magnitudes of fluvial morphological changes show the best relationship with the magnitude of peak discharge. However, during flash floods, it is difficult to perform sediment transport or bedform migration measurements to detect the timing of topographical changes, i.e. whether the greatest changes occur for example due to the peak discharge, the slope of the rising limb, or the length of the receding limb. Thus, the timing of the morphological changes during the different phases of flow hydrographs is still unresolved, and how they differ from the gravelly perennial

15 rivers, with case studies reporting most erosion during the rising and the peak flow phases of perennial rivers (e.g. Gendaszek et al. 2013).

Conventionally, these ephemeral river channel changes associated with specific flood events are interpreted on the basis of the post-flood bedform and grain size distribution (e.g. Euler et al., 2017). The only way to gain information and to show any

20 concepts about topographical changes during the flash floods is to apply simulation methods. Simulations may provide information about the channel dynamics from the times when it has not been possible to perform measurements (Lotsari et al., 2014) and thus increase our understanding of sediment dynamics during flood events (Hooke et al. 2005). However, morphodynamic simulations of gravel migration have so far been more common in perennial rivers (e.g. Williams et al., 2013) or laboratory flumes (Kaitna et al., 2011) than in ephemeral rivers. There are examples of simulating sediment transfer in

25 ephemeral channels (Graf, 1996), although most of the few recent simulations of ephemeral rivers have been performed in sandy reaches (Billi, 2011; Lucía et al., 2013) and on alluvial fans (Pelletier et al., 2005). Ephemeral rivers with gravel-sized bedload particles have seldom been simulated. One of the few existing examples was carried by Hooke et al. (2005), simulating morphological changes during flash floods with a cellular automata model.

30 It is possible to calibrate the morphodynamic model based on the between and after flood topographies. This causes uncertainties to the modelling, but it is the best available way to get understanding on the temporal evolution of the ephemeral river channels during flooding. In particular, the differences and similarities in model performance between different flood magnitudes can be detected. Recently, the measurement techniques for deriving this calibration data for morphodynamic

modelling have increased. One of them is accurate laser scanning (mobile and terrestrial), which enables to capture the channel topography before and after flooding in detail (Calle et al., 2015). Mobile laser scanning, for example from car, backpack and boat, provide practical scanning angle to survey channel banks, bar lobes and vertical surfaces, and also data collection over large channel bars has been enhanced with the method (Vaaja et al., 2011; Kasvi et al., 2015; Kukko et al., 2015). Digital

5 elevation models produced from LiDAR data have been applied for detecting the geomorphic effects of different discharge events (Hauer and Habersack, 2009; Croke et al., 2013; Thompson and Croke, 2013; Nardi and Rinaldi, 2015) and for recording and calibrating sediment transport models (Rodriguez-Lloveras et al., 2015). These reveal the reorganization of the channel morphology due to flood events even over large areas with great detail (Thompson and Croke, 2013). These accurate topography data, together with RTK-GPS measurements, enable more detailed analysis of the morphodynamic model than

10 before. Despite these advances in measurement techniques and simulation approaches, there is a need for testing the model performance in comparison to the detailed measurements related to flow events of different magnitudes, and not only to high/large floods. In addition, morphodynamic models are suited with a range of sediment transport equations to further test for simulating moderate and small floods of ephemeral channels.

15 This paper analyzes the capabilities of morphodynamic modelling for resolving the evolution of a gravelly ephemeral river channel during consecutive, moderate- and low-magnitude, discharge events. We pursue for schematic concepts for simulations in ephemeral gravely rivers that provide an outcome with the closest similarity to the post-flood reality. This study is based on both accurate topographical measurements with RTK-GPS survey and mobile laser scanning, before and after each discharge event, and morphodynamic simulation (Delft 2D). Thus, model is calibrated with data from two flash flood events.

20 Based on the simulations, we analyze the morphodynamic evolution to find out when and to what extent the channel changes occur during the different phases of discharge events, and what influence the discharge has on the rate of morphodynamics. With this simulation method it is possible to improve and deepen the analyses earlier made based on only the survey work (e.g. Calle et al., 2015).

2 The study area

25 Rambla de la Viuda is an ephemeral stream with a catchment area of 1523 km^2, located in eastern Spain (Fig. 1). The river has braided pattern associated to a high sediment supply (Calle et al., 2015). The river is prone to flash floods, and the stream flow occurs on an average of 20 days per year. Due to the high infiltration and sporadic nature of rain events, only intensive rains, i.e. a run-off threshold of 65 mm, cause flow in the river corridor (Segura-Beltrán and Sanchis-Ibor, 2013). This run-off threshold may vary between seasons, due to soil moisture and the frequency of rains.
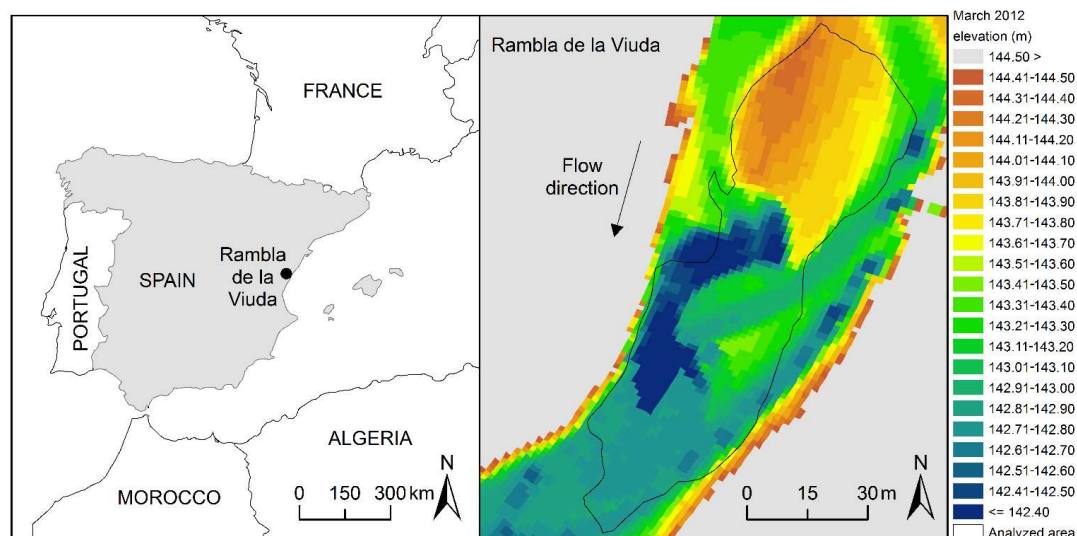
Figure 1: The study site of the Rambla de la Viuda, Eastern Spain. The elevation on March 2012 is derived mainly from mobile laser scanning data, but the edges are from the 2009 national digital elevation model. The analyzed area was defined, based on the data coverage of March 2013.

The study site is located 8 km upstream of the dam of the María Cristina reservoir. The simulation area is circa 440 m long (length along the channel) and includes an advancing gravel lobe bar front, which is the lowest 200 m of the simulation area where this study will be focused on (Fig. 1). This area was selected essentially because it was possible to assess the gravel movement with certainty (Calle et al., 2015). This is due to the gravel extraction / mining in recent decades, which has produced

10   a flat valley bottom on which gravel bars were deposited. Recently, new bars have been deposited by floods, and gravel lobes with a sharp front have been formed in the downstream edge of the area. The gravel bars and lobes of the simulation area are non- or weakly-armoured (see also Table 2) and move freely during low-magnitude flows.

The two events under study occurred in spring 2013. Even though peak discharges of 23 (on 6th March) and 12.5 m^3 s^{-1} (on 1st
15   of May) were registered in the gauging station of Vall D'Alba, respectively, the peak discharges on the study site were estimated to be greater than that due to the rain occurring between the study site and the observation stations (Calle et al. 2015). Event flows lasted 13 and 9 days, respectively. These two discharge events transported 12–41 mm sized gravel (D_{50} values). The movement of these gravels caused the development of the bar fronts (Calle et al., 2015).
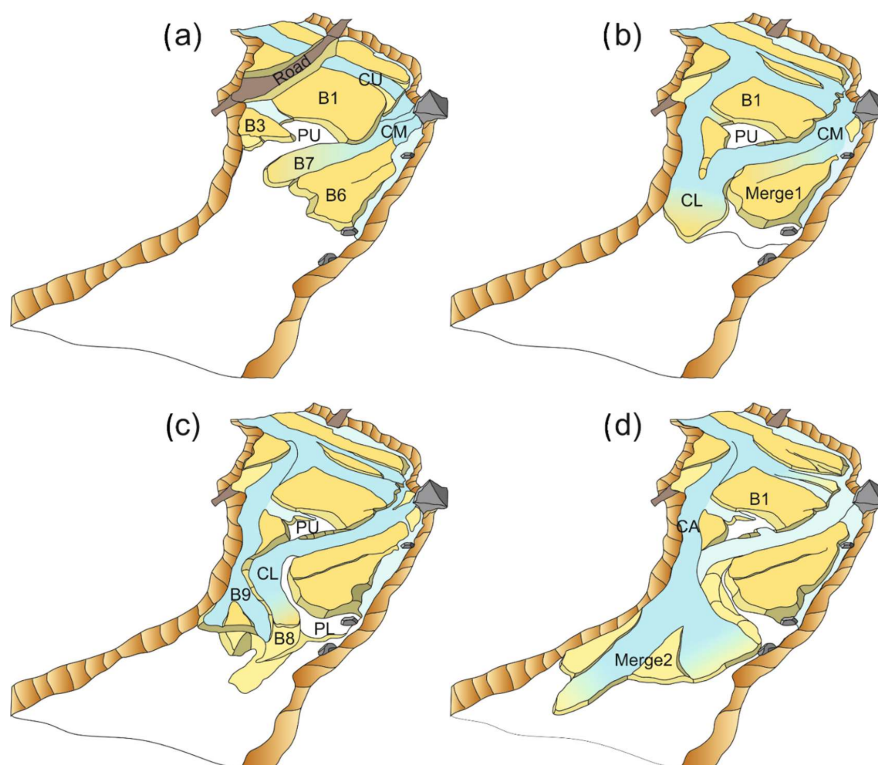
Figure 2: The conceptual graphic presented by Calle et al. (2015: Figure 10, www.schweizerbart.de/journals/zfg): the pre-stage of 2012 (a), high flood stage during March 2013 event (b), low floor stage during May 2013 event (c) and final stage after May 2013 (d). CU: Upper Channel, CM: Middle Channel, CL: Lower Channel, PU: Upper Pool, PL: Lower Pool, B1-9: gravel Bars (cf. Calle
5 **et al., 2015).**

Calle et al. (2015) described the main morphological and topographic changes in the same river reach caused by these moderate (March 2013) and small (May 2013) discharge events based on multi-temporal mobile laser scanning (MLS) and RTK-GPS
10 surveys before and after the floods (Fig. 2). They also related the observed morphological and sediment textural changes with hydraulic parameters (flow velocity, depth and discharge) estimated by a two-dimensional hydrodynamic model (Delft 2D) and investigated whether the combination of the applied techniques is a reliable method to study the morphodynamics of a flood event. It was shown that MLS surveys and additional RTK-GPS surveys are suitable for a dryland river environment. In addition, a two-dimensional hydrodynamic simulation was able to estimate the hydraulic characteristics associated with the
15 discharges. Change detection and grain size distribution analyses after flood showed a high availability of material (up to D_{84} of 32–45 mm) and absence of a well-developed armoured layer (Calle et al., 2015). Thresholds for sediment transport were

proven to fit with the Hjulström graph (1935) in this ephemeral environment. However, simulations did not include topographical change and its influence on the water level and hydraulic parameters during the floods, and could not answer how sediment transport and topographic changes evolved during rising limb, peak stage and receding limb of the hydrographs. In this paper, we investigate the modelling further for answers to those questions and deepening the analyses based on only

5   with topographical measurements.

3 Morphodynamic simulation approach

3.1 Boundary conditions: discharges and water levels

Two flow hydrographs recorded in 2013 were defined as the upstream boundary condition and the water levels as the downstream boundary condition for the hydro- and morphodynamic model (2D module of Delft3D-flow). Due to the absence

10   of direct discharge measurements at the study site, discharges recorded every 5 minutes at the gauge station of Vall d'Alba (Located 18 km upstream from the study site) were used. Also daily discharges were calculated from these 5 minutes measurements. The high-water marks (HWMs) left by the March 2013 discharge event provided evidence that the peak discharge was greater at the study site than that measured at Vall d'Alba. Thus, the discharges for the study site were re-scaled to match the peak discharge calculated during the calibration procedure of the model (see Sect. 3.4 below, and from Calle et

15   al., 2015).

Water level (hereafter WL) was defined, based on the actual HWM measurements along the longitudinal profile (Calle et al., 2015). The HWM measurements varied slightly along the longitudinal profile and the trendline, which was fitted between these measurements, showed the slope of the water surface better. The downstream-most value of this WL trendline was

20   applied as the peak WL value of March 2013 discharge event (Fig. 3, and see also Sect. 3.4). The changes in WL over time were calculated based on the relative change (%) of the discharge between each discharge measurement time interval. The WL curves for both the March and May 2013 discharges were defined and used as the downstream boundary conditions.
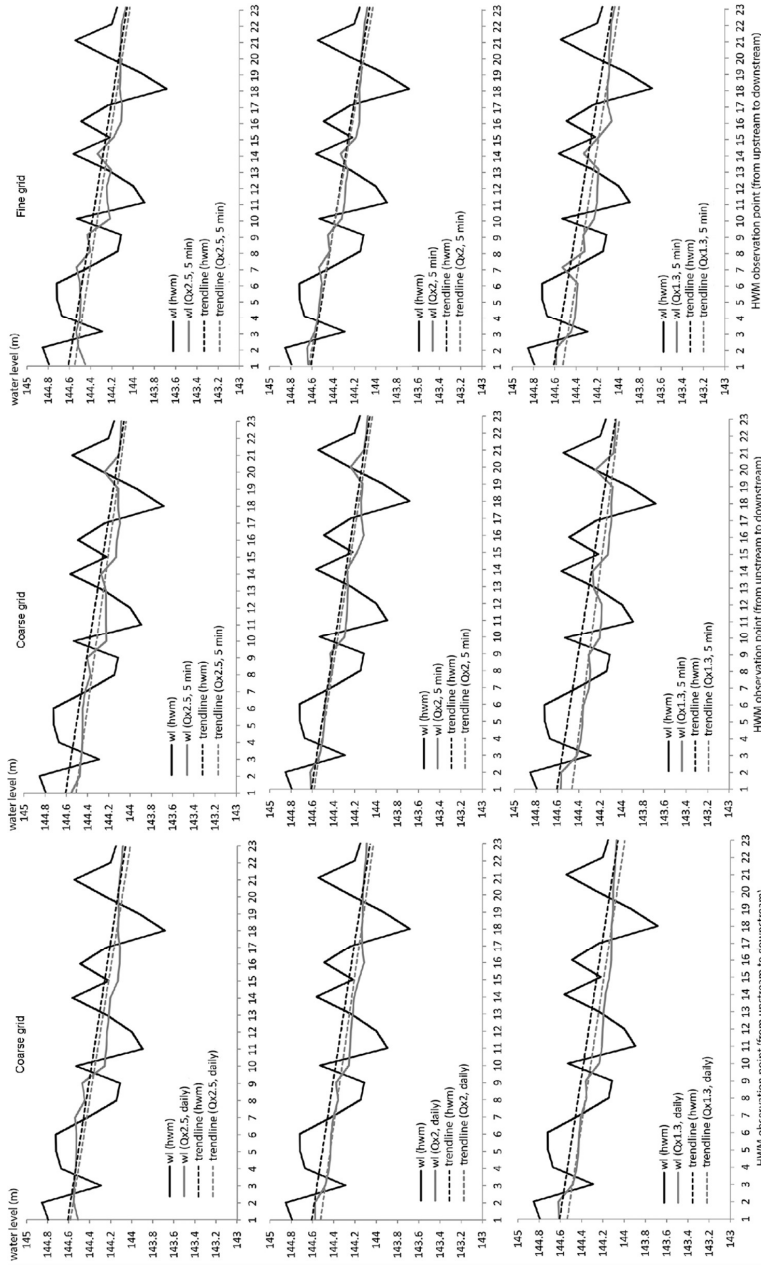
Figure 3: The hydrodynamic calibration results based on the coarse grid (1.51–5.31 m cells) and fine grid (0.76–3.03 m cells). These calibration results of the fine grid were previously presented in Calle et al. (2015) by the same authors.

3.2 Channel geometry

The channel topography was measured, using mobile laser scanning (MLS) and RTK-GPS (Calle et al. 2015). These three topography data sets were applied as 1) initial topography (March 2012), 2) calibration topography between the floods (March 2013), 3) final calibration topography after the floods (June 2013). The MLS was performed in March 2012 (pre-flood

5   situation) and in June 2013 (after the two discharge events of spring 2013) (Calle et al., 2015 and Table 1). The MLS was performed, both with a backpack and on a platform mounted on a 4x4 vehicle. A detailed description of the MLS data set can be found in Calle et al. (2015) and Table 1. According to Calle et al. (2015) and Kukko et al. (2015) the RMSE in elevation was 18.2 mm, and it was 36 mm for the 3D position of the targets. In addition, the edges of the bar lobes, which had been moved by the March 2013 discharge event, were measured with RTK-GPS just after the discharge event in March 2013

10   (Trimble 4700, 1 Hz, accuracies specified by the manufacturer: XY 0.02 m, Z 0.05 m, absolute systematic measurement error ≤ 0.054 m). This RTK-GPS data thus represented the geometry after the March 2013 event and before the May 2013 event, and was therefore also applied as a calibration data set. This enabled better estimation of the model performance than only using one calibration data set after the two consecutive flood events.

15   The Delft 2D morphodynamic model requires channel geometry in grid format. Orthogonalized curvilinear grids of two different resolution were created from both measured topographies, one with "coarse" 1.51–5.31 m cells and one with "fine" 0.76–3.03 m cells (i.e. circa half of the coarser grid cell sizes). These cell sizes were selected for testing the impacts of cell sizes on simulation results, but also due to their computational effectiveness. Cells finer than 0.76–3.03 m did not make more difference to the results, thus no further finer cell sizes were included in this paper. Furthermore, cells finer than 0.76–3.03 m

20   would have also highly increased the computational time. Thus, curvilinear grids of two resolutions, "coarse" 1.51–5.31 m cells and "fine" 0.76–3.03 m cells, were created from the topography measurement times.

Table 1. The properties of the MLS measurements of 2012 and 2013 (adapted from Calle et al. 2015).

	2012 March	2013 June
Laser sensor / GPS sensor	FARO Photon 120	FARO Focus 3D 120 S
Receiver	NovAtel DL4+	NovAtel Flexpak6
Inertial measurement unit	Honeywell HG1700 AG11	Northrop-Grumman UIMU-LCI
IMU frequency	100 Hz	200 Hz
Referencing system	GPS (1 Hz)	GNSS (1 Hz)
Wavelength	785 nm	905 nm
Scan frequency	61 Hz	95 Hz
Point acquisition	488 Hz	488 Hz
Angular resolution	0.045º (0.8 mrad)	0.07º (1.2 mrad)
3D RMSE	0.034m	0.019 m

25   The initial input channel topography for all of the Delft 2D simulations was defined by adding the MSL 2012 measurement points to the curvilinear grids, both coarse and fine grids (see above), and averaging the point values for the grid cells. There

was also available a digital elevation model (DEM) from 2009 (from airborne LiDAR), which has a 1 m resolution. After adding the MLS data, this 2009 DEM was added to the grid cells, which located outside the laser scanning perimeter, in order to cover the higher banks. The coarser resolution of the 2009 DEM did not affect the simulation results of the channel, because the high-water levels of the 2013 spring events barely reached these higher bank elevations.

For calibrating the modelling results, the topgraphies were also created from the March 2013 and June 2013 measurements so that those geometries had similar resolution as the initial input channel geometry. The model outputs after each of the discharge events were then compared to these grids created from the March and June 2013 measurements. The grid-form geometry of March 2013, i.e. calibration topography between the floods, was created by adding only the GPS measurements to the grid

10 cells, and the rest of the channel was excluded from the area to be analyzed (Fig. 1). The grid-form geometry of June 2013, i.e. the final calibration topography after the two floods, was defined by adding first the laser scanning data set, which had been processed to include both backpack and car MLS data, to the grid cells. Then the 2009 DEM was added to the grid to cover the higher bank areas. However, only the same area, as applied in the case of March 2013 (i.e. the gravel bar lobes area), was used in the final analyses of morpholocial change detection and comparison of the model performance.

These calibration curvilinear grids of "between floods" and "after floods" situations were used for analysing the capabilities of the model to result correct channel bed elevations. These simulated and measured bed elevations were compared. For volumetric calculations, these curvilinear grids and the model outputs from the same time steps were also converted into regular grids. To minimize the errors, a 0.5 m regular grid's cell size was selected, as the original cells were mostly divisible by that

20 value.

3.3 Grain sizes

Spatially varying grain sizes were measured from the gravel lobes area prior to the first flood and between the floods, using the Wolman (1954) sampling method (Table 2). However, this method did not recover the differences between upper layer and sublayer sediment distribution and what kind of particles the 2013 discharge events had in reality moved. We were able

25 to measure these only after the discharge events had occurred. Therefore, the gravel moved by the 2013 spring events were measured using a US standard gravelometer (US SAH-97 handheld particle analyzer) in summer 2014 (Table 2). These measurements represent different active forms, from bars to the channel bed, which had evolved during the 2013 spring floods. The bulk sieving measurements (c. 80 kg from 1.1x1.1 m area, 0–10 cm from the surface) were performed at six different locations, and from both the upper layer (UP1–6) and sublayer (SUB1–6, c. more than 10 cm below the surface) to evaluate

30 armouring (Table 2). The difference in the average D50 values between 2012 (18.5 mm) and 2014 (21.1 mm) measurements was only 1.6 mm (Table 2).

The D$_{50}$ and D$_{84}$ grain sizes of 2012 and March 2013 were first used for the calibration and initial testing of the hydrodynamic model (see Sect. 3.4). For the calibration of the morphodynamic model, the spatial distribution of the D$_{50}$ grain sizes of both 2012 and 2014 were then applied. The grain size values were assigned to equivalent morphological elements defined in the geomorphological map. These grain sizes were transferred to each cell of the curvilinear morphodynamic model's grid.

5   Different input grain size distributions were applied in the model tests: 1) spatially varying upper layer grain sizes, 2) spatially varying sublayer grain sizes and 3) constant average grain sizes (average of upper layer, sublayer or both upper layer and sublayer). The values were applied to the whole active layer of the river bed.

Table 2. The grain sizes measured in 2012–2014. WCM, WCU and WB1–7 were measured in 2012, WB8 and 9 were measured

10   in March 2013, and SUB1–6 and UP 1–6 were measured in June 2014. W= Wolman, C= channel, B=Bar, SUB=sublayer, UP=upper layer. Most of the samples were within the analyzed area, and their locations can be seen in Figure 11 of Calle et al. (2015). Only the samples UP/SUB 5 and 6 were further in the upstream section of the simulation area. Due to the spatial scarcity of the 2013 measurements (only two samples) were not applied as the surface grain sizes for the model, but were used for Limerinos (1970) calculations. The armour ratio was calculated following Lisle and Madej (1992), i.e. ratio of the surface-

15   to-subsurface D$_{50}$.

	upper layer		sub layer	
Sample	*D50 (mm)*	*D84 (mm)*	*D50 (mm)*	*armour ratio*
WCM	18	29	-	-
WCU	30	101	-	-
WB1	22	41	-	-
WB2	17	33	-	-
WB3	17	34	-	-
WB5	12	21	-	-
WB6	17	37	-	-
WB7	14	22	-	-
WB8	18	35	-	-
WB9	20	31	-	-
UP1 and SUB1	22.5	-	18.5	1.216
UP2 and SUB2	35.5	-	21.3	1.667
UP3 and SUB3	18.8	-	14.3	1.314
UP4 and SUB4	18.0	-	14.4	1.250
UP5 and SUB5	31.2	-	18.6	1.677
UP6 and SUB6	41.2	-	16.7	2.467
Average UP1–6	26.3	-	-	-
Average SUB1–6	17.1	-	-	-
Average UP and SUB1–6	21.1	-	-	-

3.4 Hydrodynamic simulations

The same calibrated hydrodynamic model (2D version of the Delft3D-FLOW) was applied as in Calle et al. (2015). The flow was simulated as depth-averaged flow by using the well-known Navier-Stokes and shallow-water equations. Thus, the modelled fluid was considered vertically homogeneous. These well-known equations can be found in the user manual of the

model (Deltares, 2011). The model applies the alternating-direction implicit (ADI) time integration method for the shallow-water equations (Leendertse, 1967).

The hydrodynamic model was calibrated by adjusting the Manning's n-values so that the simulated water levels matched with

5 the measured high-water level marks, and their WL trendline, of the 6.3.2013 discharge peak situation (Fig. 3 and Calle et al., 2015). The hydrodynamic model was calibrated by applying first daily discharge values as the upstream boundary condition. The n-values were defined based on Limerinos (1970) equations for D_{50} and D_{84} grain sizes (Table 3). It is noteworthy that there was no vegetation in the river channel area affecting the two (moderate and small) discharge events, and therefore the roughness values were possible to define by the particle size on the active river channel. The Limerinos equation was applied

10 for the whole range of water levels (i.e. hydraulic radiuses) for the March 2012 and March 2013 grain sizes of D_{50} and D_{84}. These represented the best of the preceding conditions of the March 2013 and May 2013 flows. The Limerinos calculations were performed for a cross-section located at the downstream side of the simulation area. This cross-section was defined from 2012 geometry, i.e. pre-flood geometry, which remained unchanged during the 2013 discharge events. At the 144.151 m water level, which was the measured high-water mark elevation at this location, the wetted perimeter of the cross-section was 52.09

15 m and the hydraulic radius was 0.95 m (max flow depth 1.28 m). Each of the geomorphological elements, and thus also grid cells, received their own Manning's n-value during the calibration procedure.

Table 3. The Manning's n-values and discharges that gave the best simulation results when compared to the measured HWMs and their trend line during the calibration. Qx1.3, Qx2 and Qx2.5 stand for Vall D'Alba's discharges multiplied by 1.3, 2 and

20 2.5, respectively. This same table is presented in Calle et al. (2015).

Element type	n (Qx2.5)	n (Qx2)	n (Qx1.3)
Channel/active bar	0.03–0.04	0.05–0.053	0.063–0.065
Extract area	0.03	0.06	0.07
Block	0.05	0.058	0.068
Exposed area	0.033–0.04	0.06	0.07
Scarce vegetation bar	0.035–0.04	0.055	0.065
Vegetated bar	0.04	0.06	0.07
Pleistocene terrace	0.05	0.06	0.07
Rocky bank	0.035	0.06	0.07
Vegetated bank	0.05	0.06	0.07
Opencast mine	0.04	0.06	0.07

The calibration was first done for the coarser grid of 1.51–5.31 m cell sizes. Because the discharge estimated at the study site was greater than the one recorded at the Vall d'Alba gauge station, three different daily discharges ("Qx1.3", "Qx2" and "Qx2.5") were tested during the calibration of the hydrodynamic model. The "Qx1.3" was defined based on the increase in

25 watershed area (30%) between the study area and the Vall d'Alba observation station. This Qx1.3 discharge simulation matched the high-water level marks using the highest n-values calculated with the Limerinos 1970 equation, i.e. for shallow

flow (Table 3). In this Qx1.3 discharge, each of the observations was multiplied by 1.3. The "Qx2" (observations multiplied by 2) water surface elevation matched the HWMs using an average n-values calculated from Limerinos (1970) equations. Also, the effects of bedform (from +0.01 to +0.015) and bank roughness (+0.02) had been added to these average n-values (Chow, 1959; Acrement and Schneider, 1989). The simulated water levels also matched with HWMs when the "Qx2.5"

5   discharge and n-values representing the high-flow stage values (i.e. lower n-values on the value range) calculated from Limerinos (1970) equations were selected. Similar n-value ranges were gained for different water level situations, when either the equation for D_{84} or D_{50} grain sizes was applied.

When the calibration against the HWMs and their trendline was successful with these daily discharges and coarse grid, the

10 same Manning's n-values were applied for simulations with a hydrograph with a 5-minute measurement interval. The "Qx1.3", "Qx2" and "Qx2.5" versions of these 5-minute hydrographs were tested. These simulations also reproduced the water levels sufficiently well, and thus no more modifications were performed for the Manning's n-values. All in all, the best fit was obtained with "Qx2" (Table 3). Finally, the 5 min hydrograph simulations were also performed with the more detailed grid, i.e. the fine grid with 0.76–3.03 m cells (Fig. 3). The hydrodynamic simulation results with the fine grid cells were better than

15 with the coarse grid cell sizes, as also shown in Calle et al. (2015).

In addition, both March and May 2013 discharge events were tested in the final hydrodynamic simulations. Similar multipliers (Qx1.3, Qx2, Qx2.5) and Manning values were applied for both events. Both these hydrographs of 2013 were simulated as an unsteady simulation and by applying the bathymetry derived from 2012 topographical measurements. The Qx2 discharge was

20 proven to best produce the observed hydrodynamics (Fig. 3; see also Calle et al., 2015). All in all, 21 hydrodynamic simulations were run during the calibration of the hydrodynamic model.

3.5 Morphodynamic simulations

Calibration of the morphodynamic model consisted on the adjustment of the model parameterization so that the model output geometries matched the first order bedform geometries as well as possible. The model applies an "upwind" bed update scheme,

25 where the elevation of the bed was dynamically updated at each computational time step. In all simulations, the initial boundary conditions of the input and output sediment transport load amount was defined as 0. This is because the flood events started from 0, and no significant transport, i.e. evolution of bedforms was observed upstream and downstream of the simulation area. The model then calculated the transport based on the selected transport equations and using equilibrium concentration. The simulation area begun further upstream than the actual analyzed area, so that sediment transport input in

30 the study reach was steady. Altogether, 61 morphodynamic simulations were needed for calibrating the morphodynamic model. These 61 simulations included simulations with Qx1.3, Qx2 and Qx2.5 discharges hydrographs. While performing the calibration, the sensitivity of the model to the different parameter combination was analyzed.

Out of these 61 morphodynamic simulations, 11 simulations, which produced the best and most interesting results, were selected to be presented in detail in this paper for sensitivity analyses (Tables 4 and 5). Due to the better performance with Qx2, all these selected morphodynamic simulations have these input data. All simulations with Qx1.3 and Qx2.5 discharges were discarded as those did not reproduce the correct topographical changes. The 11 selected simulations showed the effects

5   of grain size (before [2012] and after [2014] floods, and grain sizes from different layers [2014]), grid size (coarse: 1.51–5.31 m, fine: 0.76–3.03 m), transverse slope (user defined coefficients in the bed load transport equations: default 1.5 and increased to 3) and transportation equations (Engelund-Hansen [EH], Meyer-Peter and Müller [MP]) on model performance (Tables 4 and 5). These parameter tests were selected for the calibration procedure, as these have earlier been found important for Delft 2D model simulations, albeit in perennial rivers (e.g. Kasvi et al., 2014). The morphodynamic simulation results were

10   compared to the measured topographies (Figures 4–6), in particularly the volumetric change of river bed and displacement of the lobe front (Table 6).

Table 4. The morphodynamic simulations and applied parameters. The fine grid size is 0.76–3.03 and the coarser size is 1.51–5.31 m.EH=Engelund-Hansen, MPM=Meyer-Peter and Müller. Events: 1=only the March 2013 event has been simulated,

15   2=both the March and May 2013 events have been simulated. The simulations that were selected for the hourly channel change analyses are in bold.

Simulation	Transport equation	Discharge events	transverse slope	grid size	grain size
1	EH	1	1.5	coarse	varying, 2012
2	EH	1	1.5	fine	varying, 2012
3	EH	1	1.5	coarse	varying, upper, 2014
4	EH	1	1.5	coarse	varying, sub, 2014
5	EH	1	1.5	coarse	varying, average upper+sub, 2014
6	EH	1	1.5	coarse	constant, average upper, 2014
7	EH	1	1.5	coarse	constant, average sub, 2014
8	EH	1	1.5	coarse	constant, average upper+sub, 2014
9	**EH**	**2**	**3**	**fine**	**varying, upper, 2014**
10	**EH**	**2**	**1.5**	**fine**	**varying, upper, 2014**
11	MPM	2	1.5	fine	varying, upper, 2014

Because the bed level gradient affects the bedload transport, the slope in the initial direction of the transport (referred to as the longitudinal bed slope) and the slope in the direction perpendicular to that (referred to as the transverse bed slope) were utilised.

20   The transverse slope affects transport towards the downslope direction (Deltares, 2011). The Bagnold (1966) equation was applied for the longitudinal slope and Ikeda (1982), as presented by Van Rijn (1993), was applied for the transverse slope. The longitudinal slope was tested with both the default value (1.0) and double the default value (2.0). However, the longitudinal slope did not affect the results, and it was decided that the default value 1.0 would be used in the selected simulations, which are shown in Tables 4–6. Due to the great effects caused by the transverse slope on the morphodynamic simulations of perennial

25   rivers (e.g. Kasvi et al. , 2014), we were particularly interested in the effects of this transverse transport component on the

ephemeral river simulation, and thus tested the model with the component being 3.0, which is double the default value (1.5). These values were defined based on earlier publications (e.g. Kasvi et al., 2014).

Table 5. The simulations used for comparing the effects of different parameters on model performance. x = parameter tested in the simulation.

Simulation	Tested parameters					
	grid size effect	grain size effect: before (2012) & after flood (2014)	grain size effect: different layers	grain size effect: constant vs. varying	transverse slope effect	transportation equation effect
1	x	x				
2	x	x				
3	x	x	x			
4			x			
5			x	x		
6			x			
7			x			
8			x	x		
9					x	
10	x	x			x	x
11						x

The bedload transport was tested initially with the Van Rijn 1993 equation (VR), which is widely used, despite the fact that it was developed with smaller grain sizes than those of the study area. Also, small flow depths may affect the performance of the VR equation (Van Rijn, 1984). The depths of the flow were relatively shallow at the Rambla de la Viuda, in comparison to the channel width. As expected, the channel bed did not evolve at all with VR equation. Thus the VR equation was discarded at once (not included in Tables 4 and 5). Instead, the widely applied equations of "Engelund-Hansen 1967" (EH) and "Meyer-Peter and Müller 1948" (MPM) were selected from the Delft 2D model's assortment of equations (cf. Deltares, 2011), because they had been developed by using initially non-armoured bed conditions and were the most appropriate for the study area, according to the D_{50} grain sizes. Also, MPM has previously been proven to perform well, i.e. better than, for example, Bagnold 1980, in flash flood simulations (Reid et al., 1996; Cao et al., 2010). The MPM was expected to perform the best, as it has originally been developed for particles of 0.4–29 mm overall diameters. Earlier simulations done for ephemeral rivers, e.g. Hooke et al (2005), have applied the Bagnold (1966) total load equation. However, it was not included in the set of equations provided by the standard Delft 2D model, and thus it was not applied in this study. Instead, the EH was selected as the total load equation, due to its proven performance in a variety of environments (e.g. Kasvi et al. 2014), even though it has originally been tested on up to 0.93 mm median particle sizes (Engelund and Hansen, 1967).

Two simulations, which show after calibration the best correspondence with the observed riverbed changes and bed formations, were selected for the final channel evolution analysis. Based on these two simulations, the temporal evolution of the riverbed was analyzed during the two hydrographs of moderate- and low-magnitude discharge events.

4 Morphodynamic simulation results

4.1 The morphodynamic model's sensitivity to the parameterization

4.1.1 Effects of applied grain size on simulation results

The grain size and its spatial variation affected the model results greatly and needed the largest number of tests during the
5 calibration of the model (Tables 4–6, Figures 4–6). This was first analyzed by comparing the measured and simulated topographies and volumetric changes produced by the March 2013 flow. When the spatially varying upper layer sediments (representing the sediments actually moved by the two discharge events, i.e. the ones measured after floods in 2014) were used in the simulation (number 10), the volumetric changes were less and fitted the observations better than if spatially varying "before floods" grain sizes of 2012 were applied (simulation 2). The effects of spatially varying sublayer grain sizes (simulation
10 4) and spatially varying upper layer grain sizes (simulation 3) were compared: the deposition increased by 352 m³ when applying spatially varying sublayer grain sizes. The bedforms were also represented better with upper layer sediments. When the spatially varying average grain sizes (average of the upper and sublayer grain sizes) were applied, the simulation (number 5) resulted in a slightly greater deposition than with spatially varying upper layer grain sizes (simulation 3, Table 6). When the constant grain sizes were applied (simulation 8), the deposition was greater and resembled the observations better than a
15 corresponding simulation with spatially varying grain sizes (simulation 5), but the erosion was also greater and thalweg was excavated too deep with constant grain sizes (simulations 6–8). Altogether, the spatially varying upper layer grain sizes (measured in 2014), which were known to have been moved by the discharge events, resulted in the most realistic results.

Table 6. The evaluation of modelled volumetric changes and lobe movement, in comparison to observations. Based on the
20 performance analyses of the model during March 2013 event's simulations, the May 2013 discharge event was only simulated with a fine grid cell size, and using upper layer sediments measured in 2014 (cf. Table 4). The simulations that selected for the final hourly channel change analyses are bolded. Gravel storage was calculated by subtracting the erosion from deposition.

simula-tion	grid size	1. peak (March 2013)				2. peak (May 2013)			
		erosion (total m³; difference compared to observed %)	deposition (total m³; difference compared to observed %)	Gravel storage (total m³; difference compared to observed %)	lobe move-ment (m)	erosion (total m³; difference compared to observed %)	deposition (total m³; difference compared to observed %)	Gravel storage (total m³; difference compared to observed %)	lobe move-ment (m)
observed	coarse	89.116; 0	1252.066; 0	1162.95; 0	58.5				
observed	fine	154.564; 0	984.721; 0	830.157; 0	58.5	63.669; 0	1087.594; 0	1023.925; 0	87.1
1	coarse	267.558; +200	1071.393; -14	803.835; -31	40.6				
2	fine	286.240; + 85	1332.001; +35	1045.761; +26	69.4				
3	coarse	204.457; +129	878.286; -30	673.829; -42	47.9				
4	coarse	155.742; +75	1230.629; -2	1074.887; -8	47.9				
5	coarse	204.460; +129	992.506; -21	788.046; -32	47.9				
6	coarse	210.668; +136	992.720; -21	782.052; -33	47.9				
7	coarse	210.277; + 136	1245.116; -1	1034.839; -11	42.5				
8	coarse	185.326; +108	1106.058; -12	920.732; -21	40.23				
9	**fine**	**164.688; +7**	**1119.282; +14**	954.594; +15	**59.9**	**182.532; +187**	**1222.317; +12**	**1039.785; +2**	**61.3**
10	**fine**	**178.686; +16**	**1190.846; +21**	1012.16; +22	**52.1**	**160.090; +151**	**1289.383; +19**	**1129.293; +10**	**79.5**
11	fine	6.498; - 96	30.382; -97	23.884; -97	3.7	31.136; -51	58.139; -95	27.003; -97	3.7
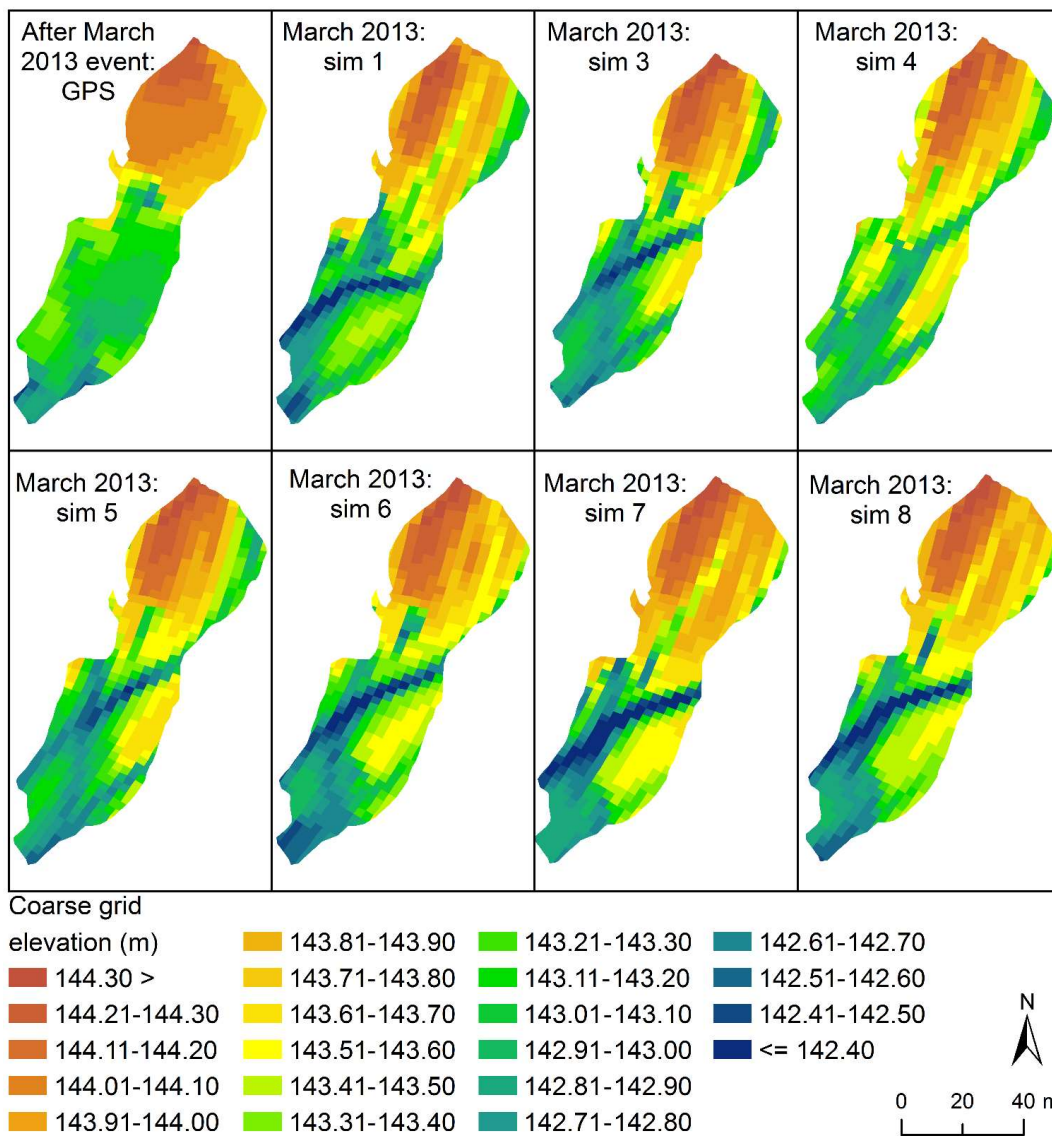
Figure 4: The bed elevations after the first March 2013 flow event (see simulation parameters from Table 4). The comparisons of the channel-bed elevations of the "analyzed area" (see Figure 1). The coarse grid cell sizes were applied in these simulations.

Figure 5: The bed elevations after the March and May 2013 flow events: The fine grid cell sizes were applied (see simulation parameters from Table 4). The comparisons were made against the bathymetries made, based on March 2013 GPS survey and June 2013 laser scanning data of the "analyzed area" of Figure 1.
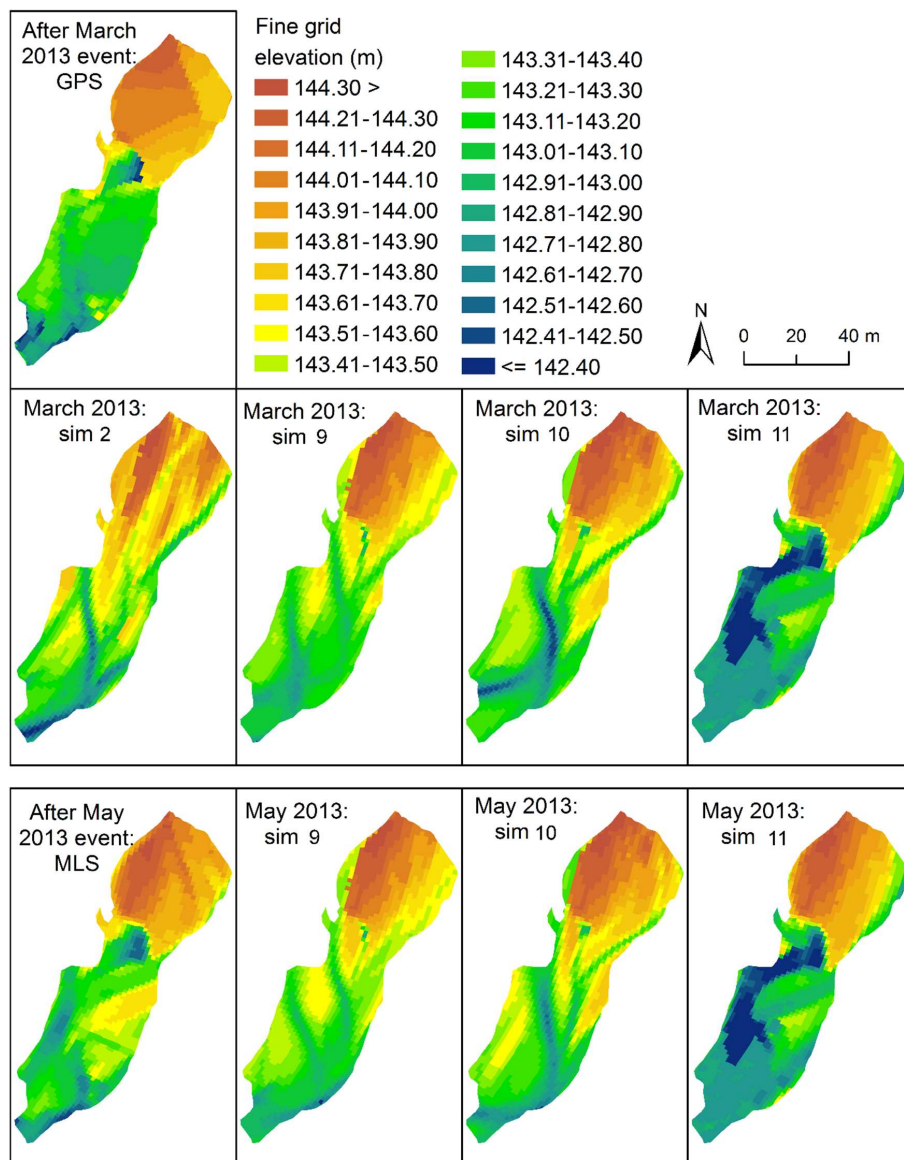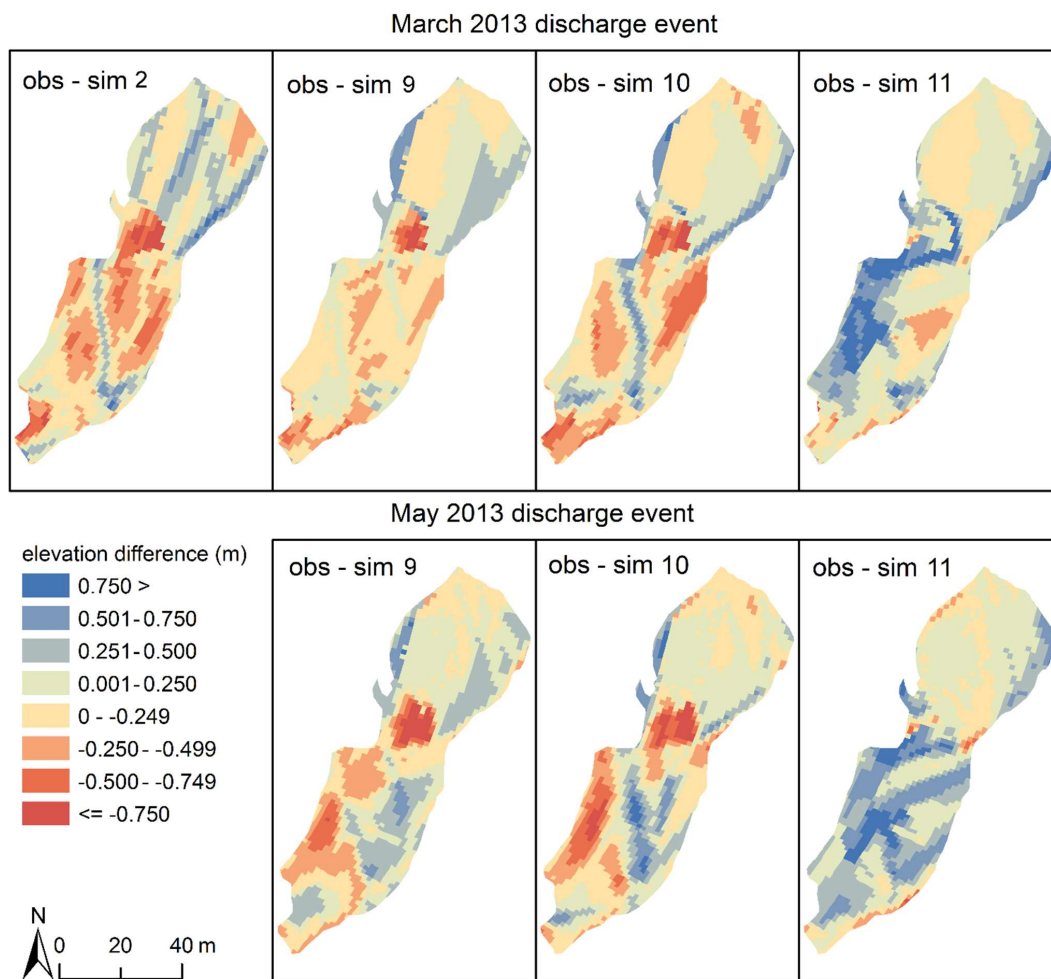
Figure 6: The comparison between the observed and simulated elevations after the March 2013 and May 2013 discharge events. The negative values (red) mean that the simulated elevations were higher in those locations. The fine grid cell sizes were applied in these simulations.

4.1.2 Effects of grid size on simulation results

The grid size effects on the simulation results were compared between simulations 1 and 2, and simulations 3 and 10 (Tables 4–6, Figures 4–6). The fine grid size tends to overestimate both erosion and deposition, whereas a coarser grid size overestimates incision. When compared to the observed topographic river bed model, the coarse grid simulations show also

an underestimation in the depositional amounts. The coarse grid also caused a moderate magnitude flood to flow mostly on the left bank side, which was opposite to the fine grid simulations and reality. The best simulation results (from the simulations 1, 2, 3 and 10) in relation to the surveyed volumetric changes were achieved with the fine grid simulation (number 10). It was decided to discard the coarse grid from the simulations of the May 2013 discharge event, and from further analyses.

4.1.3 Effects of transverse slope on simulation results

The increased transverse slope affected positively the simulation results (simulation 9), when they were compared to the corresponding simulations with the default 1.5 transverse slope (simulation 10) (Table 6, Figures 5–6). The deposition and erosion amounts resembled the observations more, when the transverse slope was increased (Table 6). The lobe movement distance was also the best with an increased transverse slope (simulation 9). Noticeable from the elevation difference analyses is that the simulations with an increased transverse slope resulted in the greatest correspondence to the observed elevations (Fig. 6). However, particularly one location in these simulations had experienced more deposition than observed: the pool area downstream of the large lateral bar (PU: Figure 2 and Calle et al., 2015).

When compared to the geomorphological evolution described in Calle et al. (2015) and the measured topographies, the spatial bedform pattern was visually compared for both the discharge events. Of all simulations, the best results were obtained with these simulations number 9 and 10. However, the default 1.5 transverse slope resulted in a more excavated thalweg (simulation 10), when compared to the simulation with an increased transverse slope (simulation 9) (Figures 5–6). However, simulation 10 also showed satisfying bar accretion from the left-bank side of the channel.

4.1.4 Effects of transport equation on simulation results

Based on the comparisons of observed and simulated topographies and volumetric changes (Table 6 and Figure 4–6), the transport equation had a crucial role in the simulation results. The EH equation (simulation 10) was superior in reproducing the channel morphology. MPM resulted in much smaller transport values (simulation 11) during both March and May 2013 discharge events (simulation 10). Basically, no movement occurred when the MPM equation was used. Thus, the MPM equation was proven not to be able to produce the correct movement during the moderate- or low-magnitude discharge events of this ephemeral gravel river.

4.2 The temporal evolution of Rambla de la Viuda

4.2.1 The evolution during moderate-magnitude flood hydrograph

Hydrographs and erosion and deposition rates were plotted against time for the simulations 9 and 10 (Fig. 7), which had reproduced the observed morphodynamics the best (see Sect. 4.1). The bed elevations from the key time steps, i.e. times of clear changes in discharge or bed evolution, are also shown (Fig. 8: simulation 9 as an example). Sediment erosion and

deposition were calculated from the total channel bed change amount of each hour. During this moderate flow event, the channel evolved and bar lobes advanced on both sides of the large lateral bar, due to the diverted flows (B1 location of Fig. 2, and Figs. 4–6 and 8). However, the main flow and bar lobe movement occurred on the right bank side of the channel and diagonal bar aggradation took place downstream part of the study site.

Both simulations experienced more deposition than erosion. The greatest erosion and deposition (m^3) occurred at the beginning of the discharge event (Fig. 7). However, the initial changes were slightly smaller when the default transverse slope was applied (simulation 10). Significant changes were observed in small peaks at 9h and 71h, which give an idea of the high system response to steep changes in the discharge, rather than a progressive increase (as seen in the absolute peak of 23h). The

10 deposition in simulations 9 and 10 started very slowly decreasing after 13 hours, but the decrease in erosion was slightly faster. However, all in all, the deposition and erosion remained high for a long time and only started clearly declining after 71 hours, i.e. the secondary discharge peak. The erosion and deposition volumes followed the changes in receding discharge more faithfully than during the rising phase, occurring simultaneously to the changes in discharge. Thus, the morphodynamics of both simulations 9 and 10 followed the changes in discharge better during the falling stages of the discharge peak, i.e. when

15 the discharge was 30 m^3 s^{-1} or less. During the rising phase, there were temporal differences between changes in discharge and changes in deposition and erosion. When the default transverse slope was applied (simulation 10), the erosion and deposition continued to be high longer in the receding phase than when the transverse slope was increased to 3 (simulation 9). The great deposition amount during the receding phase was mainly due to the propagation of the bar lobe front.

4.2.2 The evolution during low-magnitude flood hydrograph

20 During the May discharge event, the changes in erosion and deposition followed the discharge evolution more than during the March discharge event (Fig. 7). The main flow path was again on the right bank side of the channel, where the greatest changes also occurred. The discharge event of the May 2013 had two peaks, of which the latter discharge peak was greater. The erosion and deposition peak occurred approximately an hour after this greatest peak discharge had been reached. Thus, the deposition and erosion peaks did not occur immediately at the beginning of the discharge event, as in the case of the March 2013 event.

25 The erosion became greater than the deposition four hours after the beginning of the discharge event (simulation 9). Six hours after the sediment transport peak (at 25 h), the deposition dominated again. During the March discharge event, the erosion was never greater than the deposition. Note also that the discharge remained constant after both peaks, whereas a decrease in the deposition and erosion rates was observed.
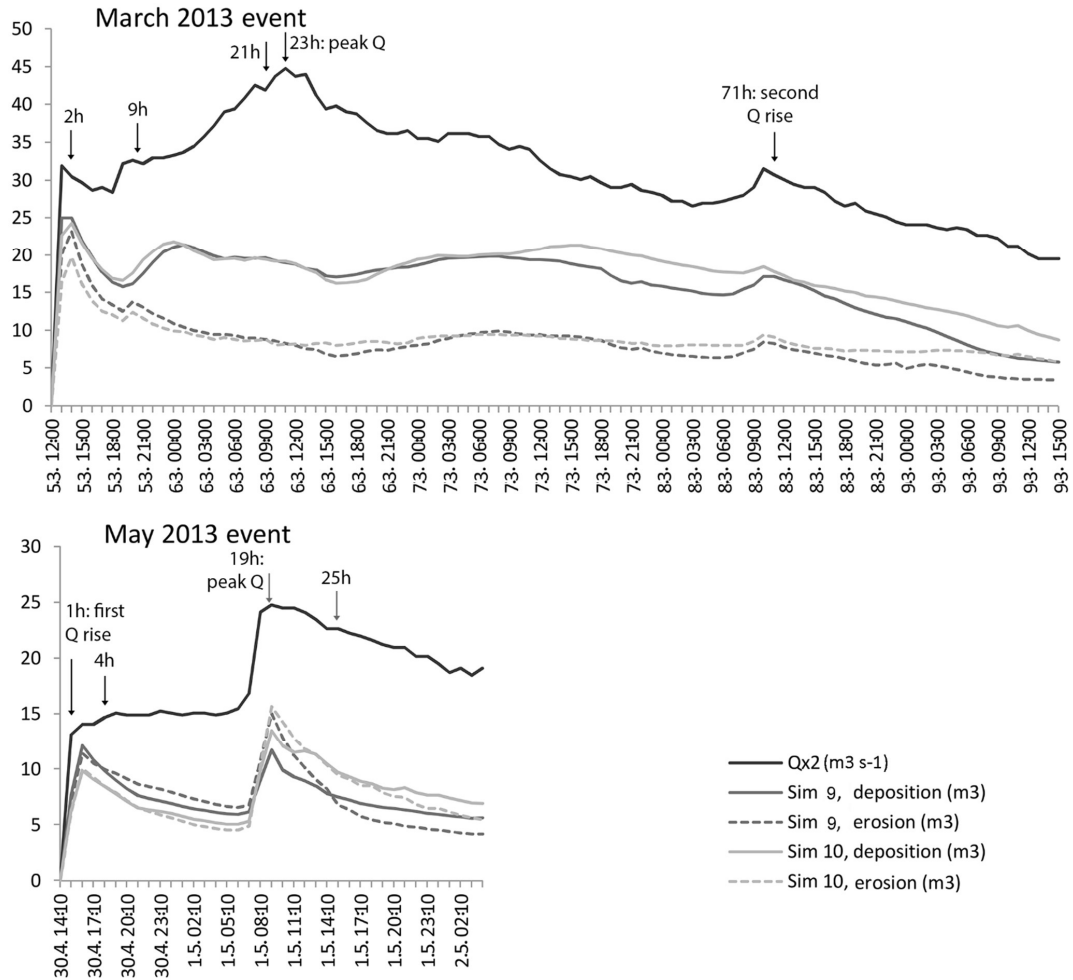
Figure 7. The hourly volumetric changes during the moderate- and low-magnitude flow events of March and May 2013. The results are based on simulations 9 and 10. The graphs show the erosion and deposition from the beginning of the flow events (12:00 on 5th March and 14:10 on 30th April) until the time when the erosion and deposition had declined and levelled out during the receding phases. The important points of time are pointed out as hours from the beginning of the flow events.
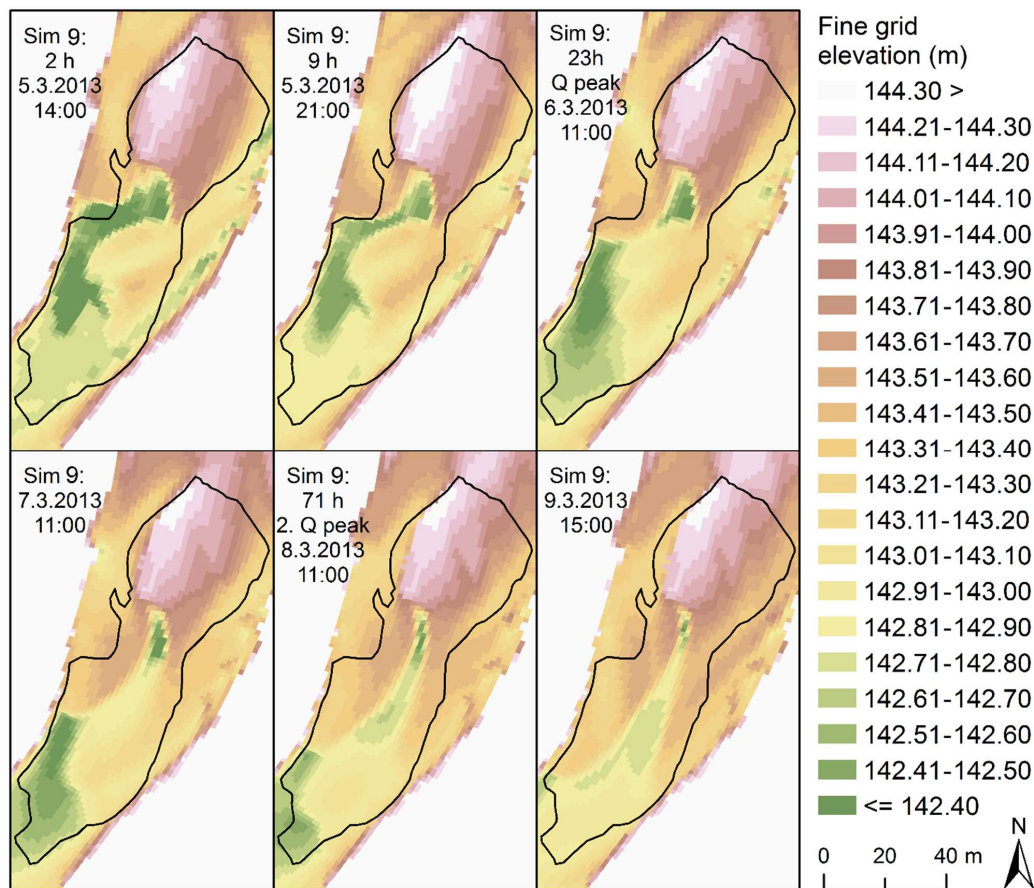
Figure 8. The bed elevations of simulation 9 (with increased transverse slope) during moderate discharge event. The key time steps are presented (cf. Figure 7).

5 Discussion

5.1 Uncertainties related to the simulations

The morphodynamic simulation of the ephemeral river provides a good quantification of the sequence of channel changes described by Calle et al. (2015). It also deepens the analyses done based on only the topographical data, and is the only way to gain concepts about topographical changes during the flash floods. The reliability of the model results improves with the quality and temporal density of the available calibration topography, i.e. between and after flood bedform geometries. We had

two topographical calibration data sets, which is more than in many other studies. However, we think that further research with multiple yet-to-come events needs to be run to assess the repeatability and validation of the model even better. Transport rates and flow velocity measurements would be suitable to calibrate models during the event, but they are always difficult and dangerous to perform in this particular environment. The uncertainties related to this have to be acknowledged. However, as

5 the forefront lobe prograded over a flat valley bottom (as gravel bed had been mined), we had a good control on sediment volume and gravel particle-size moving downstream. In fact, the bedload sediment output from the studied reach was zero. In addition, the simulation result supports the hypothesis of Calle et al. (2015) that moderate- and low-magnitude events reworked sediment locally. This means that these flows were not able to establish a sediment connection upstream and the transported sediment originated from the erosion of adjacent areas. In addition, we were able to use a discharge station further upstream

10 of the study area, and thus also a hydrograph with a known shape. Sometimes only the high water marks are known, and for example, Cao et al. (2010) analyzed the bedload transport by using a symmetrical hydrograph. This could be why their simulations showed less transport during the receding phase than ours.

As the curvilinear girds of fine 0.76–3.03 m and coarse 1.51–5.01 m cells were tested for morphodynamic simulations, the

15 finer grid was proven to better predict the channel evolution, including both flow and bar lobe movement paths. Furthermore, the grain sizes and their spatial distribution affected the morphodynamic simulation results greatly. Hooke et al. (2005) have shown that grain sizes have a major effect on the morphological impacts of floods. Simulation results may be enhanced when using techniques that are able to obtain spatially more complete and detailed grain size data (such as Wang et al., 2013) from the surface layers, instead of lower resolution site sampling, such as Wolman method. Parker (1990) stated that a calculation

20 of the bedload transport rate of mixtures should be based on the availability of each size range in the surface layer. The best simulation results of Rambla de la Viuda were indeed gained when spatially varying upper surface layer sediment sizes were applied. However, further detailed analyses of spatial and vertical grain size distribution effects on ephemeral gravel-bed river morphodynamic simulations are suggested. Next step should be to apply the surface grain size variation derived from the laser scanning data sets (Casas et al., 2010a and b; Kukko et al., 2015).

According to Kasvi et al. (2014), the transverse bed slope parameterization affects the sediment transport in the downslope direction particularly in long-term simulations. However, also during these rather short-term flood event simulations at gravelly Rambla de la Viuda, the effects of the increasing transverse slope on channel evolution was evident, and the simulation results resembled more the observed topographies. Kasvi et al. (2014) had noticed that the model run with a high transverse bed slope

30 effect (i.e. value 3) predicted more filling of the pool in an meandering river, when compared with the model run with no transverse bed slope effect. Similarly to Kasvi et al. (2014), the pool area of Rambla de la Viuda had experienced more deposition with the increased transverse slope value. This pool area was the only clearly wrongly simulated location with this higher transverse slope value, but otherwise the lobe movement and elevation resembled the best to the observations, when this high transverse slope value was applied. Thus, in a gravel bed river with short lasting flow events, adjustments are clearly

needed in this parameter for being able to replicate the observed changes while simulating with the currently available sediment transport equations. Thus, similarly to the perennial river simulations (e.g. Kasvi et al., 2014), the transverse slope was important for the simulated changes.

5   Earlier, Hooke et al. (2005) and Graf (1996) have applied the Bagnold equation to an ephemeral channel, but we wanted to use the equations that have often been used together with the Delft 2D model. Reid et al. (1996) showed that the Meyer-Peter and Müller (MPM, 1948) equation, which was originally developed for steady flow conditions and used by Reid et al. (1996) in non-armoured gravel bars, performs well and better than the Bagnold (1980) and Parker (1990) equations in ephemeral gravel river channels. This justified the application of the MPM equation in the ephemeral gravelly Rambla de la Viuda. Reid

10   et al. (1996) stated that the reason for this is partly due to the fact that sediment was not supply-limited by channel-bed armour development, which is the case in many perennial rivers. However, the movement was minimal with the MPM equation and occurred only in the beginning of the moderate event. The second discharge event could not cause much movement with the MPM equation, even though movement had occurred based on the field measurements. The MPM equation is a deterministic equation. According to Van Rijn (1993), in a strongly decelerating flow, the deterministic formulae do not give realistic results

15   because the mean bed-shear stress approaches zero in the case of flow separation and reattachment, and thus sediment transport also approaches zero. This may have happened in the Rambla de la Viuda, as the MPM equation did not move particles anymore during the receding phase of the hydrographs. The application of the deterministic MPM equation could also partly explain why the receding phase's transport was less according to Cao et al. (2010) than based on the present study.

20   According to Barry et al. (2004) the formulae containing a transport threshold typically exhibit poor performance when compared to the observed gravel bed river's bed load data. These equations include MPM (1948) and Bagnold (1960) equations, which have been applied in ephemeral channels. Barry et al. (2004) noted that simulation results done with different sediment transport equations show substantial differences in performance, but no consistency has been found between equation performance and the complexity of the equation. Despite being unable to produce the correct morphodynamics caused

25   by the moderate- or low-discharge events of Rambla de la Viuda, the MPM equation could have potential in the simulation of greater floods of ephemeral gravelly rivers, similarly as Reid et al. (1996) and Cao et al. (2010) have shown.

Engelund and Hansen (1967) developed their equation, so that the effects of dunes, e.g. transport from stream-side to lee-side and form drag, were included. This could be the reason why the EH worked the best at the Rambla de la Viuda, where clear

30   sharp lobe edges occur, and the local slope varies a lot. In addition, the EH is a total load equation (Engelund and Hansen, 1967), whereas, for example, the MPM equation calculates bedload. Meyer-Peter and Müller (1948) equation applies an energy slope, which, for example, Van Rijn (1984) has stated not to be an appropriate parameter for morphological mathematical modelling. The disadvantages of the use of the energy gradient may be according to Van Rijn (1984) the variations due to non-

equilibrium phenomena of rising and falling stages. This could partly explain why the EH worked better than the MPM in this ephemeral river.

5   However, despite the challenges of applying morphodynamic simulation approaches to ephemeral river channel change analyses, the results are promising, and show the importance of both rising and receding phases. The observations of sediment transport during flow hydrographs would still be important, in addition to the continuous time series of pre- and post-flood topography, but at the moment, their measurement is still a complex and risky issue. By continuing the long-term observations of the ephemeral channel changes with the high-precision equipment, more reliable calibration and validation of the models may be gained.

10   **5.2 Moderate- and low-magnitude flow events as channel modifiers**

Our study has shown that geomorphic responses in ephemeral rivers, such as Rambla de la Viuda, are unique to each discharge event, and the model needs to be calibrated based on consecutive discharge events, and not just one event. Previously this uniqueness to the response has been shown for perennial rivers (Pitlick, 1993). The methods and conceptual results of this present study can be applicable in ephemeral rivers worldwide (e.g. USA, House and Pearthree, 1995). Hooke (2016a) stated

15   that the flow events of similar magnitude can have differing effects, depending on the state of the system, as the long-term evolution of the ephemeral river channel and its material greatly influence the response to the stream flow. Some events are more erosional and some are more depositional (Hooke, 2016a). Moreover, Hooke et al. (2005) noted the importance of simulating and analysing the feedback effects of consecutive events. At Rambla de la Viuda, the riverbed morphology formed by the March 2013 influenced the later channel changes during the May 2013 flow. For example, the flow was diverted to the

20   right bank side during the first flood (of March 2013), which also therefore acted as the main channel for the May 2013 flow, which was lower in magnitude.

The model was calibrated based on the observations before/between and after the discharge events, because it is knowingly impossible to measure during the risky flash flood events, albeit moderate and low in their magnitude. Therefore, the following

25   discussion is purely based on the model outputs.

The simulation results of the Rambla de la Viuda showed that the differences between rising, peak and receding phases of a moderate-magnitude discharge event are very important in an ephemeral river environment. Higher total amount of channel changes occurred during the receding phase than at the early stages of the discharge events. Deposition dominated due to the

30   progradation of the frontal bar lobe, particularly on the right bank side of the channel. Thus, the continuous channel changes were similar to those for braided perennial rivers (Lotsari et al., 2014). However, this differs from a recent study of Gendaszek et al. (2013), who studied the gravel perennial riverbed changes during moderate- (65 m^3 s^{-1}) and high-flow (159 m^3 s^{-1}) events.

They found that most erosion occurred during the rising and the peak flow phases, but did not mention great changes during the receding phase.

Ferguson stated already in 1993 the potential in numerical modelling of the coupling between geometry, flow, and bedload
5   transport, if it can be applied successfully for the braided channels. The results were promising at Rambla de la Viuda, which also has a braided pattern. According to Wheaton et al. (2013) the chute cutoff mechanism, already described by Ferguson (1993), is the most common braiding mechanism, but that the cutoff is not only an erosional process, but more the result of deposition during the construction of diagonal bars. In the study area of ours, there was a situation resembling to chute cutoff, as the channel was cut more on the right bank side of the bar than before. The modelling was capable in producing this observed
10   chute cutoff from the right bank side during the moderate discharge event (March 2013). Both erosion and deposition related to these changes, as both topographical observations and model simulations showed the development of the diagonal bar alongside with the cutoff of the bar. However, the diagonal bar formation was slightly greater in the model outcomes than based on observations. Despite this, the model showed potential in producing the channel development following the established theories of gravel bed evolution. In addition, the model showed that the initial cutoff and simultaneous initiation
15   of the diagonal bar took place during the rising limb, but the diagonal bar would not have developed to its full extent without the long receding phase of the flood hydrograph.

Noteworthy is that during the moderate-discharge event the erosion and deposition peak occurred much earlier than the discharge peak. However, the low-magnitude discharge event experienced the greatest channel changes an hour after the
20   discharge peak. Our model results (e.g. Figs. 7 and 8) suggest the existence of hysteresis in the rate of bedform changes, being clockwise or positive in the case of moderate-magnitude flow (bedform change peak occurs before flood peak), and negative in the case of low-magnitude flow (bedform change peak occurs during/after flood peak). The hysteresis phenomenon has been described well in sediment transport studies, and their effect is due, among other factors, to sediment depletion or surface gravel consolidation in the channel (Reid et al., 1985) or a long-lasting portion of the baseflow during the recession limb
25   (Walling, 1974). Cao et al. (2010) have shown, based on their 1D simulations, that bedload transport in an ephemeral river can have similarities to a perennial river. However, even though perennial rivers may have sharp rising phases in their discharge hydrographs (e.g. Long, 2009), they more likely have a greater initial threshold for particle movement by bed-armouring than ephemeral rivers (Reid et al., 1996; Hassan et al., 2009). Although, their armouring can though decrease as bed load concentrations increase (Müller and Pitlick, 2013). Hysteresis of both kinds have also been shown in perennial rivers regarding
30   turbidity, but their flashy storm hydrographs have more often caused anti-clockwise (i.e. negative) hysteresis phenomenon (Lloyd et al., 2016). This would indicate that ephemeral rivers act more similarly to perennial rivers during their low magnitude flow events. Even though further research is needed, the results indicate that the greater the discharge event's magnitude in an ephemeral river is, the more different the channel evolution and its timing are compared to perennial rivers.

These hysteresis phenomena show a time dependence on the fluvial system outputs, depending on a previous sediment transport size and gravel bar morphology, which affects the internal state and the future morphodynamic response. In our study reach, 30 m^3 s^{-1} was the threshold discharge for the channel changes to become gradual and to follow the discharge changes during the receding phase. According to Hooke (2016a), the threshold values of hydraulic conditions for erosion and deposition

5   in ephemeral channels vary between sites, mostly due to the size and nature of the bed material. Threshold discharge has been observed to be for the deposition and erosion of 15 mm particles 35 m^3 s^{-1} and 1 m^3 s^{-1}, respectively, and of 50 mm particles 14 m^3 s^{-1} and 40 m^3 s^{-1}, respectively (Hooke, 2016a). The average upper and sublayer D_{50} grain sizes at the Rambla de la Viuda were 26.3 mm and 17.1 mm, respectively, and the maximum D_{50} grain size was 40.2 mm. The discharges of the Rambla de la Viuda were overall within the ranges of Hooke's thresholds for the movement of these-sized particles, and the simulations

10   clearly showed their transport. In addition, the threshold discharge of 30 m^3 s^{-1} for starting the channel changes of the Rambla de la Viuda to follow the discharge changes during the receding phase coincide well with Hooke's (2016a) threshold analysis of deposition.

6 Conclusions

Due to the proven morphological changes caused by low- and moderate-magnitude discharge events, the preventive measures

15   against flash flood-induced channel changes should take into account moderate- and low-magnitude flows. This has received support from earlier studies (e.g. Hooke, 2016a and b). As the receding phase can cause substantial channel changes, it plays a major role in inducing damages/modifications to the river environments, and it needs to be acknowledged while planning flood mitigation measures. We have demonstrated the goodness of 2D modelling for analysing ephemeral river channel changes. The following schematic concepts can be concluded about the morphodynamics and their simulations in an ephemeral

20   river during moderate- and low-magnitude discharge events:

1) The morphodynamic 2D model was proven to work in an ephemeral river affected by flash floods. Instead of applying calibration data from only one discharge event, the model results can be enhanced by applying topographical pre- and after flood data from consecutive flood events. When modelling events of moderate and low magnitude in rivers of 50 to 100 meters wide, a resolution of at least 1m is recommended (i.e. one cell is 1–2 % of the total width). At Rambla de la Viuda, the

25   curvilinear grid with mesh edge lengths of 0.76–3.03 resulted topographically more realistic outcomes than with coarser grid of i.e. grid size 1.51–5.31 m. A coarser resolution results in incorrect flow and sediment transport routing, as the edges of the bar lobes are smoothed, which affects simulation of water level, hydraulics and bed form evolution. The finer grid was able to show the steep lobes forefront scarp and showed that laser scanned data is the way to produce the detailed scale topography for simulating the bar lobe movement. Otherwise, procedures would need to include manual modification of the topography

30   to include the lobe edges.

2) 2D morphodynamic models can be a good approach for shedding light on the temporal evolution of channel evolution during flash flood events, as measurements during flash floods are risky to perform. With simulations it is possible to improve

and deepen the analyses earlier made based on only the survey work or hydrodynamic modelling, as it is possible to analyze whether the greatest changes occur for example due to the peak discharge, the slope of the rising limb, or the length of the receding limb of the flood hydrograph.

3) The spatially varying grain size data, the applied transverse slope parameter value and sediment transport equations are the

5   most important factors, apart from the quality of recorded discharge, for the simulation results of the channel evolution. The total load equation worked better, compared to the deterministic equation.

4) Both rising and receding phases of discharge events were predicted to be important for bar movement and channel evolution and thus should not be ignored while planning flood mitigation measures. The erosion and deposition can be greater during the long-lasting receding phase than at the rising phase of moderate- and low-magnitude discharge events, despite the typical

10 hydrograph shape of a flash flood. The receding phase contributed also greatly on the shaping of the bed forms and channel pattern.

5) The deposition and erosion peak rates are predicted to occur at the beginning of the moderate-magnitude discharge events (e.g. March 2013 event), whereas deposition dominates throughout the event, i.e., even during the rising phase. On the contrary, the low-magnitude discharge events (e.g. May 2013 event) only experience the greatest channel changes after the discharge

15 peak.

6) These different predicted erosion/deposition patterns suggest a hysteresis effect on the morphodynamic changes, closely related to sediment transport rates, and stress the importance of previous flood history (timing, succession and magnitude) in understanding the geomorphic response of gravelly ephemeral rivers.

7) The clearest difference in the predicted riverbed changes between the rising and receding phases is that erosion and

20 deposition characteristics follow the temporal discharge changes more during the receding phase than during the rising phase. The threshold discharge, below which the channel-bed changes started following the discharge changes temporally, was around $30 \ m^3 \ s^{-1}$. This threshold should be further tested in other ephemeral channels in Mediterranean, and elsewhere.

Data availability

The data has been stored in the universities of the authors. Due to the great size of the data, those can be accessed by request

25 from the authors. Each request will be processed separately.

Author contribution

Lotsari has done most of the writing and all of the model simulations. Calle and Benito have been also greatly contributed in the writing of the paper and have enabled the study with their projects, as they have initiated the studies of Rambla de la Viuda. All the other authors have contributed to the writing process by commenting the manuscript and its content. All authors have

30 contributed in collecting the field data. Laser scanning has been done by Kukko, Kaartinen, and Alho. The laser scanning data

has been processed by Kukko and Kaartinen. Hyyppä J. and Hyyppä H. and have contributed by providing funding for the study and they have also worked on the development of the laser scanning approaches. Benito, Calle and Lotsari have measured the sedimentological data. GPS measurements of topography and high water marks have been done by Benito and Calle.

Competing interests

5   The authors declare that they have no conflict of interest.

Acknowledgements

We would like to thank the Institut Cartografic Valencia, Servicio Automatico de Informacion Hidrologica of the Confederacion Hidrográfica del Júcar for supporting data. Financial support is provided by the Spanish "Ministerio de Economia y Competitividad" (projects CGL2011-29176 and CGL2014-58127-C3-1-R), the Academy of Finland (Extreme

10   and annual fluvial processes in river dynamics – ExRIVER [grant number 267345], the Centre of Excellence in Laser Scanning Research – CoE-LaSR [grant number 272195], and the Strategic Research Council project "COMBAT" [grant number 293389]) and Maj and Tor Nessling Foundation (Äärimmäisten ja vuotuisten fluviaaliprosessien vaikutukset jokidynamiikkaan [grant number 2013067]).

References

15   Acrement, G.J. and Schneider, V.R.: Guide for Selecting Manning's Roughness Coefficients for Natural Channels and Flood Plains, United States Geological Survey Water-Supply Paper, 2339, 1–38, 1984.

Bagnold, RA.: An Approach to the Sediment Transport Problem from General Physics. Geological Survey Professional Paper 422–I. United States Government Printing Office: Washington, 1966.

Bagnold, R.A.: An empirical correlation of bedload transport rates in flumes and natural rivers, P. Roy. Soc Lond. A Mat.,

20   372, 453–473, doi: 10.1098/rspa.1980.0122, 1980.

Barry, J.I., Buffington, J.M., and King J.G.: A general power equation for predicting bed load transport rates in gravel bed rivers, Water Resour. Res., 40, W10401, doi:10.1029/2004WR003190, 2004.

Benito, G., Thorndycraft, V.R., Rico, M.T., Sánchez-Moya, Y., Sopeña, A., Botero, B.A., Machado, M.J., Davis, M. and Pérez-González, A.: Hydrological response of a dryland ephemeral river to southern African climatic variability during the

25   last millennium, Quaternary Res., 75, 471–482, 2011.

Billi, P.: Flash flood sediment transport in a steep sand-bed ephemeral stream, Int. J. Sediment Res., 26, 193–209, doi: 10.1016/S1001-6279(11)60086-3, 2011

Calle, M., Lotsari, E., Kukko, A., Alho, P., Kaartinen, H., Rodriguez-Lloveras, X. and Benito, G.: Morphodynamics of an ephemeral gravel-bed stream combining mobile laser scanner, hydraulic simulations and geomorphological indicators, Z. Geomorphol. Supp., 59, 33–57, 2015

Cao, Z., Hu, P. and Pender, G.: Reconciled bedload sediment transport rates in ephemeral and perennial rivers, Earth Surf.
5   Proc. Land., 35, 1655–1665, doi: 10.1002/esp.2005, 2010.

Casas, A., Lane, S.N., Yu, D. and Benito, G.: A method for parameterising roughness and topographic sub-grid scale effects in hydraulic modelling from LiDAR data, Hydrol. Earth Syst. Sc., 14, 1567–1579, 2010a.

Casas, M.A, Lane, S.N., Hardy, R.J., Benito, G. and Whiting, P.J.: Reconstruction of subgrid-scale topographic variability and its effect upon the spatial structure of three-dimensional river flow. Water Resour. Res., 46, W03519,
10   doi:10.1029/2009WR007756, 2010b.

Chow, V.T.: Open Channel Hydraulics, McGraw-Hill Book Company, New York, USA, 1959.

Croke, J., Fryirs, K. and Thompson, C.: Channel–floodplain connectivity during an extreme flood event: implications for sediment erosion, deposition, and delivery, Earth Surf. Proc. Land., 38, 1444–1456. doi: 10.1002/esp.3430, 2013

Deltares: Delft3D-FLOW, Simulation of Multi-dimensional Hydrodynamic Flows and Transport Phenomena, Including
15   Sediments, User Manual: Hydro-Morphodynamics. Delft, The Netherlands, 2011.

Engelund, F. and Hansen, E.: A Monograph on Sediment Transport in Alluvial Streams, Technical University of Denmark, Teknisk Forlag, Copenhagen, 1967

Euler, T., Herget, J., Schlömer, O. and Benito, G.: Hydromorphological processes at submerged solitary boulder obstacles in streams, Catena, 157, 250–267, https://doi.org/10.1016/j.catena.2017.05.028, 2017.

20   Ferguson, R.I.: Understanding braiding processes in gravel-bed rivers: progress and unsolved problems. In: Braided Rivers, Geological Society Special Publication No. 75, edited by: Best, J. L. and Bristow, C.S., 73–87, 1993.

Gendaszek, A.S., Magirl, C.S., Czuba, C.R. and Konrad, C.P.: The timing of scour and fill in a gravel-bedded river measured with buried accelerometers, J. Hydrol., 495, 186–196. doi: 10.1016/j.jhydrol.2013.05.012, 2013.

Graf, W.L: Transport and deposition of plutonium-contaminated sediments by fluvial processes, Los Alamos Canyon, New
25   Mexico, Geol. Soc. Am. Bull., 108, 1342–1355, doi: 10.1130/0016-7606(1996)108<1342:TADOPC>2.3.CO;2, 1996.

Greenbaum, N. and Bergman, N.: Formation and evacuation of a large gravel-bar deposited during a major flood in a Mediterranean ephemeral stream, Nahal Me'arot, NW Israel, Geomorphology, 77, 169–186, doi: 10.1016/j.geomorph.2006.01.016, 2006.

Grodek, T., Jacoby, Y., Morin, E. and Katz, O.: Effectiveness of exceptional rainstorms on a small Mediterranean basin,
30   Geomorphology, 159–160, 156–168, doi: 10.1016/j.geomorph.2012.03.016, 2012

Hassan, M.A., Marren, P.M. and Schwartz, U.: Bar structure in an arid ephemeral stream, Sediment. Geol., 221, 57–70. doi:10.1016/j.sedgeo.2009.07.012, 2009.

Hauer, C. and Habersack, H..: Morphodynamics of a 1000-year flood in the Kamp River, Austria, and impacts on floodplain morphology, Earth Surf. Proc. Land., 34, 654–682, doi: 10.1002/esp.1763, 2009.

Hjulström, F.: Studies of the Morphological Activity of Rivers as Illustrated by the River Fyris. – Inaugural Dissertation, Almqvist & Wiksells, 1935.

Hooke, J.: Morphological impacts of flow events of varying magnitude on ephemeral channels in a semiarid region, Geomorphology, 252, 128–143, doi: 10.1016/j.geomorph.2015.07.014, 2016 a.

Hooke, J.: Geomorphological impacts of an extreme flood in SE Spain, Geomorphology, 263, 19–38, doi: 10.1016/j.geomorph.2016.03.021, 2016 b.

Hooke, J.M. and Mant, J.M.: Geomorphological impacts of a flood event on ephemeral channels in SE Spain, Geomorphology, 34, 163–180, doi: http://dx.doi.org/10.1016/S0169-555X(00)00005-2, 2000.

Hooke, J.M., Brookes, C.J., Duane, W. and Mant, J.M.: A simulation model of morphological, vegetation and sediment changes in ephemeral streams, Earth Surf. Proc. Land., 30, 845–866, doi: 10.1002/esp.1195, 2005.

Ikeda, S.: Incipient Motion of Sand Particles on Side Slopes, J. Hydr. Eng. Div.-ASCE, 108, 95–114, 1982.

Kaitna, R., Chiari, M., Kerschbaumer, M., Kapeller, H., Zlatic-Jugovic, J., Hengl, M. and Huebl, J.: Physical and numerical modelling of a bedload deposition area for an Alpine torrent, Nat. Hazard. Earth Sys., 11, 1589–1597, doi:10.5194/nhess-11-1589-2011, 2011.

Kasvi, E., Alho, P., Lotsari, E., Wang, Y., Kukko, A., Hyyppä, H. and Hyyppä, J.: Two-dimensional and three-dimensional computational models in hydrodynamic and morphodynamic reconstructions of a river bend: sensitivity and functionality, Hydrol. Process., 29, 1604–1629, doi: 10.1002/hyp.10277, 2014.

Kasvi, E., Vaaja, M., Kaartinen, H., Kukko, A., Jaakkola, A., Flener, C., Hyyppä, H., Hyyppä, J. and Alho, P.:Sub-bend scale flow–sediment interaction of meander bends — A combined approach of field observations, close-range remote sensing and computational modelling, Geomorphology, 238, 119–134, doi: 10.1016/j.geomorph.2015.01.039, 2015.

Kukko, A., Kaartinen, H. and Zanetti, M.: Backpack Personal Laser Scanning System for Grain-Scale Topographic Mapping, 46th Lunar and Planetary Science Conference, The Woodlands, TX, USA, 2015.

Laronne, J.B. and Reid, L.: Very high rates of bedload sediment transport by ephemeral desert rivers, Nature, 366, 148–150, doi:10.1038/366148a0, 1993.

Limerinos, J.T.: Determination of the Manning coefficient from measured bed roughness in natural channels, Geological survey water-supply paper, 1898-B, U.S. Department of the Interior, prepared in cooperation with the California Department of Water Resources, United States Government Printing Office, Washington, 1970-

Lisle, T.E. and Madej, M.A.: Spatial variation in armouring in a channel with high sediment supply, In: Dynamics of Gravel-bed Rivers, edited by: Billi, P., Hey, R.D., Thorne, C.R. andTacconi, P., John Wiley & Sons Ltd., Chichester, 277–293, 1992.

Long, A.J.: Hydrograph separation for karst watersheds using a two-domain rainfall–discharge model. J. Hydrol., 364, 249–256, doi:10.1016/j.jhydrol.2008.11.001, 2009

Lotsari, E., Wainwright, D., Corner, G.D., Alho, P. and Käyhkö, J.: Surveyed and modelled one-year morphodynamics in the braided lower Tana River, Hydrol. Process., 28, 2685–2716, doi: 10.1002/hyp.9750, 2014.

Lloyd, C.E.M., Freer, J.E., Johnes, P.J. and Collins, A.L.: Using hysteresis analysis of high-resolution water quality monitoring data, including uncertainty, to infer controls on nutrient and sediment transfer in catchments, Sci. Total Environ., 543, 388–404, doi: 10.1016/j.scitotenv.2015.11.028, 2016

Lucía, A., Recking, A., Martín-Duque, J.F., Storz-Peretz, Y. and Laronne, J.B.: Continuous monitoring of bedload discharge
5 in a small, steep sandy channel, J. Hydrol., 497, 37–50, doi:10.1016/j.jhydrol.2013.05.034, 2013.

Meyer-Peter, E. and Müller, R.: Formula for bed load transport, Proceedings of the 2nd Meeting, Int. Assoc. Hydraulic Structures Res. (IAHR), Stockholm, Sweden, 39–64, 1948.

Müller, E.R. and Pitlick, J.: Sediment supply and channel morphology in mountain river systems: 1. Relative importance of lithology, topography, and climate, J. Geophys. Res.-EARTH, 118, 2325–2342. doi:10.1002/2013JF002843, 2013.

10 Nardi, L. and Rinaldi, M.: Spatio-temporal patterns of channel changes in response to a major flood event: the case of the Magra River (central–northern Italy), Earth Surf. Proc. Land., 40, 326–339, doi: 10.1002/esp.3636, 2015.

Parker, G.: Surface-based bedload transport relation for gravel rivers, J. Hydraul. Res., 28, 417–436, doi: http://dx.doi.org/10.1080/00221689009499058, 1990.

Pelletier, J.D., Mayer, L., Pearthree, P.A., House, P.K., Demsey, K.A., Klawon, J.E. and Vincent, K.R.: An integrated approach
15 to flood hazard assessment on alluvial fans using numerical modeling, field mapping, and remote sensing, Geol. Soc. Am. Bull., 117, 1167–1180, doi: 10.1130/B25544.1, 2005.

Pitlick, J.: Response and recovery of a subalpine stream following a catastrophic flood, Geol. Soc. Am. Bull., 105, 657–670, 1993.

Reid, I., Frostick, L.E. and Layman, J.T.: The incidence and nature of bedload transport during flood flows in coarse-grained
20 alluvial channels, Earth Surf. Proc. Land., 10, 33–44. doi: 10.1002/esp.3290100107, 1985.

Reid, I., Powell, D.M. and Laronne, J.B.: Prediction of bed-load transport by desert flash floods, J. Hydraul. Eng., 122, 170–173, doi: 10.1061/(ASCE)0733-9429(1996)122:3(170), 1996.

Rodriguez-Lloveras, X., Bussi, G., Francés, F., Rodriguez-Caballero, E., Solé-Benet, A., Calle, M. and Benito, G.: Patterns of runoff and sediment production in response to land-use changes in an ungauged Mediterranean catchment, J. Hydrol., 531,
25 1054–1066, 2015.

Segura-Beltrán, F. and Sanchis-Ibor, C.: Assessment of channel changes in a Mediterranean ephemeral stream since the early twentieth century, The Rambla de Cervera, eastern Spain, Geomorphology, 201, 199–214, doi: 10.1016/j.geomorph.2013.06.021, 2013.

Thompson, C. and Croke, J.: Geomorphic effects, flood power, and channel competence of a catastrophic flood in confined
30 and unconfined reaches of the upper Lockyer valley, southeast Queensland, Australia, Geomorphology, 197, 156–169, doi: 10.1016/j.geomorph.2013.05.006, 2013.

Vaaja, M., Hyyppä, J., Kukko, A., Kaartinen, H., Hyyppä, H. and Alho, P.: Mapping Topography Changes and Elevation Accuracies Using a Mobile Laser Scanner, Remote Sens., 3, 587–600, doi:10.3390/rs3030587, 2011.

van Rijn, L. (1984). Sediment transport, part I: bed load transport. J. Hydraul. Eng., 110, 1431–1456. doi: 10.1061/(ASCE)0733-9429(1984)110:10(1431).

van Rijn, L.C.: Principles of Sediment Transport in Rivers, Estuaries and Coastal Seas, 1993 edition, Aqua Publications, The Netherlands, 1993.

5 Walling, D.E.: Suspended sediment and solute yields from a small catchment prior to urbanisation, in: Fluvial Processes in Instrumented Watersheds, edited by: Gregory, K.J. and Walling, D.E., Special Publication 6, Institute of British Geographers, 169–192, 1974.

Wang, Y., Liang, X., Flener, C., Kukko, A., Kaartinen, H., Kurkela, M., Vaaja, M., Hyyppä, H. and Alho, P.: 3D Modeling of Coarse Fluvial Sediments Based on Mobile Laser Scanning Data, Remote Sens., 5, 4571–4592, doi: 10.3390/rs5094571, 2013.

10 Wheaton, J., Brasington, J., Darby, S.E., Kasprak, A., Sear, D. and Vericat, D.: Morphodynamic signatures of braiding mechanisms as expressed through change in sediment storage in a gravel-bed river, J. Geophys. Res. Earth Surf., 118, 759–779, doi:10.1002/jgrf.20060, 2013.

Williams, R.D., Brasington, J., Hicks, M., Measures, R., Rennie, C.D. and Vericat, D.: Hydraulic validation of two-dimensional simulations of braided river flow with spatially continuous ADCP data, Water Resour. Res., 49, 5183–5205, doi: 15 10.1002/wrcr.20391, 2013.

Wolman, MG.: A method of sampling coarse river-bed material, Transactions of the American Geophysical Union, 35, 951–956, 1954.